Sensing with Chirality-Pure Near-Infrared Fluorescent Carbon Nanotubes

Robert Nißler, Larissa Kurth, Han Li, Alexander Spreinat, Ilyas Kuhlemann, Benjamin S. Flavel, and Sebastian Kruss*

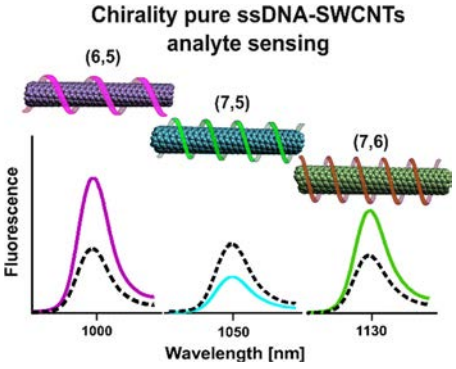

ABSTRACT: Semiconducting single wall carbon nanotubes (SWCNTs) fluoresce in the near infrared (NIR) region, and the emission wavelength depends on their chirality (*n*,*m*). Interactions with the environment affect the fluorescence and can be tailored by functionalizing SWCNTs with biopolymers such as DNA, which is the basis for fluorescent biosensors. So far, such biosensors have been mainly assembled from mixtures of SWCNT chiralities with large spectral overlap, which affects sensitivity as well as selectivity and prevents multiplexed sensing. The main challenge to gain chirality pure sensors has been to combine approaches to isolate specific SWCNTs and generic (bio)functionalization approaches. Here, we created chirality pure SWCNT based NIR biosensors for important analytes such as neurotransmitters and investigated the effect of SWCNT chirality/handedness as well as long term stability and sensitivity. For this purpose, we used aqueous two phase extraction (ATPE) to gain chirality pure (6,5) , (7,5) , (9,4) , and (7,6) SWCNTs (emission at ∼990, 1040, 1115, and 1130 nm, respectively). An exchange of the surfactant sodium deoxycholate (DOC) to specific single stranded (ss)DNA sequences yielded monochiral sensors for small analytes (dopamine, riboflavin, ascorbic acid, pH). DOC residues impaired sensitivity, and therefore substantial removal was necessary. The assembled monochiral (6,5) SWCNTs were up to 10 times brighter than their nonpurified counterparts, and the ssDNA sequence determined the absolute fluorescence intensity as well as colloidal (long term) stability and selectivity for the analytes. $(GT)_{40}$ (6,5) SWCNTs displayed the maximum fluorescence response to the neurotransmitter dopamine (+140%, $K_d = 1.9 \times 10^{-7}$ M) and a long term stability of >14 days. The specific ssDNA sequences imparted selectivity to the analytes mostly independent of SWCNT chirality and handedness of (±) (6,5) SWCNTs, which allowed a predictable design. Finally, multiple monochiral/single color SWCNTs were combined to achieve ratiometric/multiplexed sensing of the important analytes dopamine, riboflavin, H_2O_2, and pH. In summary, we demonstrated the assembly, characteristics, and potential of monochiral (single color) SWCNTs for NIR fluorescence sensing applications.

INTRODUCTION

Single wall carbon nanotubes (SWCNTs) are 1D nanomateri als with unique photophysical properties.[1−4] Semiconducting SWCNTs show fluorescence in the near infrared (NIR) region of the electromagnetic spectrum (optical tissue transparency window), which offers ultralow background and high tissue penetration.[5] The emission wavelength depends on their carbon lattice structure, described by the chiral index/chirality (*n*,*m*).[6] Because of these properties SWCNTs are versatile building blocks for NIR labels and sensors.[7−11] As nanosensors they are powerful tools to study biological processes with high spatial, temporal, and chemical resolution.[12−19] The most prominent examples are the detection of signaling molecules such as neurotransmitters,[12,20,21] reactive oxygen species (ROS),[13,14] and nitric oxide (NO).[17] Additional sensing concepts have been developed for genetic material,[15,22] lipids,[23] proteins,[24−26] and bacterial motifs.[27] Not only are such sensors able to report the presence of the molecule but also imaging of many of them allows one to get spatiotemporal chemical information.[28] Using this concept, for example, the release and secretion of the neurotransmitters dopamine and serotonin from cells could be resolved.[12,21] So far NIR fluorescent sensors based on SWCNTs have been assembled mainly from an as synthesized SWCNT material, which contains multiple chiralities, catalyst residues, and impurities. However, for the simultaneous detection of different analytes, multiple sensors with unambiguous fluorescence emission and hence SWCNT chirality are required. The synthesis of chirality enriched SWCNTs has improved over the last years, but commercially available SWCNT materials still contain multiple chiralites.[29,30] Therefore, separation and purification

approaches are required to obtain samples with well defined characteristics.[31,32] SWCNTs have been separated by density gradient centrifugation,[33,34] gel chromatography,[35−37] ion exchange chromatography,[38] and aqueous two phase extraction (ATPE).[39−41] Furthermore, certain macromolecules such as single stranded (ss)DNA sequences[42,43] or polyfluorenes (PFOs)[44] preferentially solubilize certain chiralities, which provides a route to monochiral samples. In the past years ATPE of SWCNTs has made tremendous progress in the isolation of various small and large SWCNT chiralities.[41,45−48] In this approach SWCNTs are dispersed in either a surfactant such as sodium deoxycholate (DOC) or chirality specific ssDNA[49,50] sequences and separated between aqueous phases of two different polymers. This fast, reliable, and low cost separation method appears to be an optimal starting point to obtain monochiral sensors. Unfortunately, chirality pure SWCNTs extracted by these approaches are coated with the macromolecule or surfactant used for the purification process. The surfactant can be removed, but the purer a sample becomes, the more the hydrophobic SWCNTs tend to stick to each other and redispersion in other surfactants and biopolymers becomes difficult.[51]

In contrast, the chemical design of sensors requires functionalization with biomolecules that impart specificity to the SWCNT. Chemical approaches include noncovalent functionalization with DNA,[43] peptides,[52] peptide−DNA conjugates,[53] protein−DNA conjugates,[16,54] proteins,[26] and lipids.[24,55] Recently, also sp^3 quantum defects on SWCNTs have been modified covalently with biomolecules.[56] Overall, the surface chemistry is crucial for molecular recognition and signal transduction. Some of the best studied systems so far are DNA functionalized SWCNTs that recognize small molecules. Certain sequences make the SWCNT sensitive to biomolecules: for example, to the neurotransmitter dopamine.[20,57] In this particular case, it was shown that interactions of the two hydroxy groups of dopamine with the DNA backbone cause conformational changes that lead to an increase in quantum yield.[12,58] In contrast, simple adsorption and redox chemistry could be ruled out.[58,59]

Consequently, the surface chemistry on SWCNTs is the most important part to tailor sensor properties, but this has not been explored in detail and combined with purified monochiral SWCNTs. The aforementioned difficulties have so far impaired the obvious next step to use monochiral SWCNTs as building blocks for NIR fluorescent sensors and labels.

Here, we isolate monochiral SWCNTs to assemble single color fluorescent sensors and study the effect of chirality and surface functionalization on the fluorescent sensing of biomolecules. For this purpose, we combine ATPE with surface exchange methods to ssDNA sequences (including aptamers) and polymers. The presented strategy minimizes SWCNT aggregation during surface exchange and redispersion. We quantify and compare the photophysical properties, stabilities, and fluorescence responses of monochiral and multichiral sensors. Finally, we make use of the nonoverlapping emission spectra of monochiral SWCNTs and demonstrate ratiometric and multiplexed sensing.

MATERIALS AND METHODS

All materials, if not otherwise stated, were purchased from Sigma Aldrich.

SWCNT Surface Modification. (6,5) Chirality enriched CoMoCat SWCNTs (Sigma Aldrich, product no. 773735) were modified with varying single stranded (ss)DNAs such as $(GT)_5$, $(GT)_{10}$, $(GT)_{20}$, $(GT)_{40}$, $(C)_{30}$, $(A)_{30}$, $(T)_{30}$, $(GC)_{15}$, $(GA)_{15}$, and $(AT)_{15}$ (oligonucleotide sequences purchased from Sigma Aldrich) following a previously described protocol.[59] Thereby, 100 μL of ssDNA (2 mg/mL in H_2O) was mixed with 100 μL of 2×PBS and 100 μL of SWCNTs (2 mg/mL in PBS), tip sonicated for 15 min @ 30% amplitude (36 W output power, Fisher Scientific Model 120 Sonic Dismembrator) and centrifuged 2× for 30 min @ 16100*g*. DOC dispersed SWCNTs were obtained by tip sonicating 4 mg of CoMoCat SWCNTs in 2 mL 1% DOC for 30 min @ 40% amplitude, followed by 2× 30 min centrifugation @ 16100*g*.

SWCNT Separation. The separation of (6,5) SWCNTs was performed according to a previously reported aqueous two phase extraction (ATPE) protocol from Li et al.[41] Briefly, in a three step approach SWCNT chiralities were separated between two aqueous phases, containing dextran (MW 70000 Da, 4% *m*/*m*) and PEG (MW 6000 Da, 8% *m*/*m*) with varying pH values *via* HCl addition. The final B_3 (bottom) phase yielded monochiral (6,5) SWCNTs, which were diluted with DOC to obtain a stable 1% DOC SWCNT solution. Dialysis (300 kDa dialysis bag, Spectra/Por, Spectrum Laboratories Inc.) against 1% DOC removed the dextran polymer used for SWCNT separation. The separation of (7,5) and (9,4) SWCNTs followed a pH modulated ATPE process similar to that described above. Instead of 0.05% DOC and 0.5% SDS for the normal process, 0.07% DOC and 0.5% SDS were used here to improve the resolution of (7,5) as well as (9,4) SWCNTs. (7,6) SWCNTs were obtained by using a similar ATPE method but from a different CoMoCAT raw soot (CHASM, lot #SG76 L39). Briefly a three stage ATPE process was used to sort single chirality (7,6). In stage 1, SDS concentrations were changed from 0.5% to 1.5% with a constant DOC concentration (0.04%) to get a (7,6) enriched top fraction (T_4, with SDS ∼0.7%). Then a fresh bottom phase was added to T_4, and SDS concentrations were again changed from 0.6% to 1% with the same DOC of 0.04% to further purify this enriched (7,6) fraction. In the end, a metal semiseparation was performed to remove the metallic tubes at stage 3.

Enantiomerically pure (6,5) SWCNTs were prepared by a similar diameter sorting on the basis of DOC/SDS.[39] First the concentrations of SDS 0.9% and DOC 0.04% were used in order to push all species larger than (6,5) SWCNTs to the top phase and remove them. Then the SDS concentrations were increased very slowly and step by step to 1.3%. The next seven continuous fractions (T_1−T_7) were collected, and all of them were (6,5) enriched. After the next semiconducting metallic separation, T_2 was found to be highly enantiomerically (−) (6,5) enriched. Sodium cholate (SC) was then used to further separate highly enriched (+) (6,5) from the fraction T_4. CD measurements were performed on an CD spectrometer (J 1500, JASCO) from 800 to 200 nm through a 1 mm path length cuvette in 1 nm steps (scanning speed 100 nm/min, bandwidth ∼2.2 nm).

Monochiral SWCNT Surface Exchange to ssDNA. Surface exchange of the SWCNTs toward ssDNA was achieved by applying the steps from Streit et al.[60] Purified (6,5) SWCNTs in 1% DOC were diluted to an absorbance of 2.0 at the E_{11} transition (986 nm). The concentration of (7,5) SWCNTS was 2.0 at 1032 nm, for (9,4) SWNCTs 0.9 at 1112 nm, and for (7,6) SWCNTs 1.6 at 1129 nm. A 150 μL portion of purified SWCNTs in 1% DOC was mixed with 25 μL of PEG (MW 6 kDa, 25% *m*/*v* in H_2O) and 30 μL of ssDNA (2.0

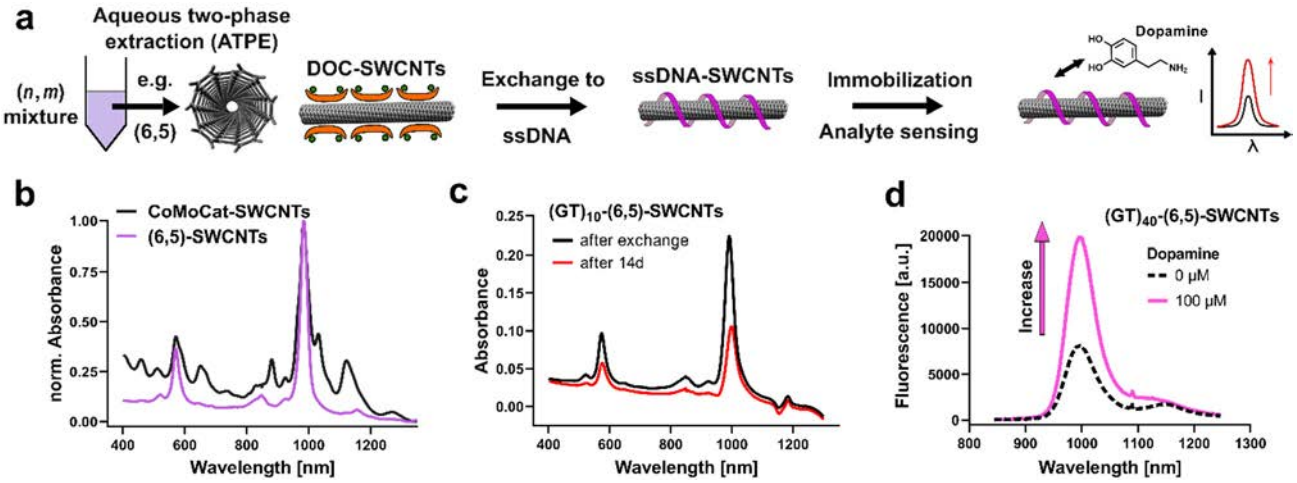

Figure 1. Assembly of chirality pure near infrared fluorescent carbon nanotube based sensors. (a) Schematic of the workflow. Aqueous two phase extraction (ATPE) yielding chirality pure SWCNTs (e.g., (6,5) SWCNTs) from a parental mixture. Exchange of the organic corona from the surfactant sodium deoxycholate (DOC) to single stranded (ss)DNA or other (bio)polymers leads to monochiral functionalized SWCNTs that serve as sensors for small molecules such as the neurotransmitter dopamine. (b) Exemplary normalized absorbance spectra of parental CoMoCat SWCNTs and purified (6,5) SWCNTs in 1% DOC. (c) Nine different ssDNA (6,5) SWCNTs were assessed. Here, exemplary absorbance spectra of $(GT)_{10}$ (6,5) SWCNTs directly after surface exchange and after 14 days are shown. (d) ssDNA SWCNTs immobilized on a glass surface and exposed to analytes that change their NIR fluorescence in a DNA sequence dependent way. Here, the exemplary monochiral fluorescence spectrum of a sensor for the neurotransmitter dopamine is shown.

mg/mL in H_2O). After one precipitation cycle, due to the stepwise addition of 270 μL of methanol and subsequent addition of 600 μL of isopropyl alcohol, the loose nanotube pellet was separated from the supernatant by short (1 s) centrifugation @ 16100*g*. The supernatant was further centrifuged for 2 min @ 16100*g*, and the obtained DNA pellet residue was redispersed in 300 μL of 1×PBS. This solution was used to redisperse the nanotube pellet by bath sonication or 10 s of tip sonication. Further centrifugation (5 min @ 16100*g*) yielded the monochiral nanosensors, which were characterized afterward by absorption spectroscopy. For stability measurements the ssDNA (6,5) SWCNTs were diluted to an absorbance at an E_{11} transition (~991 nm) of 0.2 and measured again after time intervals of 1, 3, 7, and 14 days. Surface exchange toward PEG PL (18:0 PEG5000 PE, Avanti Lipids) was performed by following a modified protocol.[55] DOC dispersed chirality pure SWCNT fractions were concentrated and washed with sodium cholate (SC, 12 mg/mL in 1xPBS) using molecular cutoff spin filtration (Vivaspin 500, 100000 Da molecular weight cutoff, Sartorius). A 800 μL portion of these SC SWCNTs was mixed with 2 mg of 18:0 PEG5000 PE dissolved in 200 μL of PBS and dialyzed 2 days against 1×PBS, using a 1 kDa cutoff dialysis tube. The final PEG PL SWCNTs were obtained after 20 min of centrifugation @ 16100*g*. For ratiometric H_2O_2 sensing, the hemin binding aptamer (HeApta) 5′ AGTGTG AAA TAT CTA AAC TAA ATG TGG AGG GTG GGA CGG GAA GAA GTT TAT TTT TCA CAC T 3′ was used,[13,61] with a concentration of 50 nM hemin.

NIR Spectroscopy. Absorption spectra were acquired with a JASCO V 670 device from 400 to 1350 nm in 0.2 nm steps in a 10 mm path length glass cuvette. 1D NIR fluorescence spectra were measured with a Shamrock 193i spectrometer (Andor Technology Ltd., Belfast, Northern Ireland) connected to an IX53 Microscope (Olympus, Tokyo, Japan). Excitation was performed with a gem 561 laser (Laser Quantum, Stockport, UK). 2D excitation emission spectra were collected with a Monochromator MSH150 instrument, equipped with a LSE341 light source (LOT Quantum Design GmbH, Darm stadt, Germany) as the excitation source.

NIR fluorescence analyte response measurements were performed by letting 60 μL of a 0.2 nM ssDNA SWCNT solution (molar nanotube concentration calculation based on previous literature[62−64]) adsorb overnight (12 h) on a glass bottom 96 well plate (#1 cover glass, 0.13−0.16 mm, Cellvis, P96 1 N), followed by washing with PBS and addition of 20 μL of the analyte to 180 μL of PBS (addition of 20 μL of 0.06 M HCl to obtain pH 6 as validated by a pH meter). NIR fluorescence spectra were acquired with 130 mW excitation @ 561 nm and 10 s integration time. D Adrenaline was purchased from AKos GmbH (Lörrach, Germany). Dose−response measurements were fitted with a one site specific binding fit (GraphPad Prism 8) using $Y = B_{max}X/(K_d + X)$ with X = concentration of the analyte, Y = specific binding; B_{max} = maximum binding, and K_d = dissociation constant.

Atomic Force Microscopy. AFM analysis was performed on an JPK NanoWizard (Bruker) instrument in tapping mode. SWCNT dispersions were drop casted on a freshly cleaved muscovite mica surface, incubated for 15 min, and rinsed with deionized H_2O. A total number of 732 individualized SWCNTs were analyzed with Gwyddion (2.53), and the corresponding descriptive statistics were fitted with a Weibull distribution (Origin 9.1).

RESULTS AND DISCUSSION

To create nanosensors with narrow emission spectra, chirality pure SWCNTs are necessary, and we used a scalable ATPE approach that yields large amounts of e.g. (6,5) SWCNTs (Figure 1a,b and Figure S1 in the Supporting Information). Exchange and variation of the ssDNA surface modification enabled the synthesis of different nanosensors, which were evaluated regarding their optical properties, colloidal stability, and sensitivity in biosensing (Figure 1c,d).

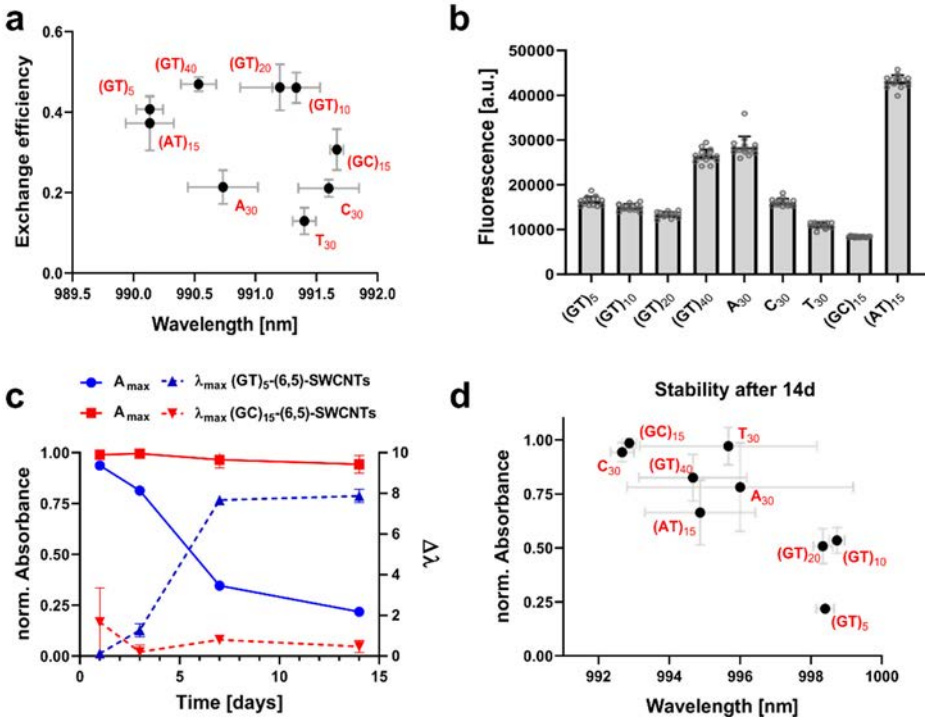

Figure 2. Surface exchange and colloidal stability of chirality pure ssDNA (6,5) SWCNTs. (a) Exchange efficiency and E_{11} absorbance maxima of nine different ssDNA (6,5) SWCNTs for surfactant exchanges to ssDNA (n = 3, mean ± SEM). All monochiral nanosensors have very similar absorbance features (maxima and FWHM of E_{11} transmission). (b) Fluorescence intensities of 0.2 nM ssDNA (6,5) SWCNTs. $(AT)_{15}$ (6,5) SWCNTs show the highest fluorescence emission (mean ± SD, n = 15, technical replicates from three independent exchange experiments). (c) Normalized E_{11} absorbance and wavelength shift evaluated after 1, 3, 7, and 14 days post (6,5) SWCNT surface exchange to ssDNA for two exemplary sequences (normalized to the absorbance at t = 0). $(GT)_5$ (6,5) SWCNTs show a decrease in absorbance and red shift, which indicate lower colloidal stability. In contrast, for example $(GC)_{15}$ (6,5) SWCNTs remain stable over weeks (mean ± SEM, n = 3). (d) Colloidal stability for different ssDNA sequences as measured by the normalized E_{11} absorbance 14 days after surface exchange (normalized to the absorbance at t = 0) (mean ± SEM, n = 3).

Impact of ssDNA Sequence on Brightness and Stability. Variation of the ssDNA sequence leads to ssDNA/SWCNT conjugates that are sensitive to different biologically important molecules.[57,65] Therefore, we first evaluated the influence of the ssDNA sequence on the surface exchange process and optical properties. For this purpose, DOC (6,5) SWCNTs (Figure 1b) of the same concentration/absorbance (Figure S2 in the Supporting Information) were exchanged to different ssDNA sequences.

A typical ssDNA (6,5) SWCNT absorption spectrum is shown in Figure 1c, and an analysis of all E_{11} absorption features for the different ssDNA (6,5) SWCNTs after surface exchange is summarized in Figure 2a. All monochiral nanosensors displayed an absorbance maximum between 990.2 nm and 991.6 nm but large differences in absolute absorption. ssDNA sequences were able to redisperse 13% (T_{30}) to 47% ($(GT)_{40}$) of the parent surfactant stabilized (6,5) SWCNTs in 1% DOC (shown as mean ± standard error of the mean (SEM)). This exchange efficiency was calculated by correlating the E_{11} absorption features (maximum absorption × FWHM) from the DOC and ssDNA solutions, similarly to the approach by Streit et al.[60] We assumed a similar absorption cross section for SWCNTs with different ssDNA functionalizations and diluted all ssDNA (6,5) SWCNTs accordingly to the same concentration (0.2 nM in PBS), but we observed strong differences in fluorescence (Figure 2b). The calculation of concentrations is based on the approach by Schöppler et al. (see Materials and Methods).[64] It accounts for spectral features of SWCNTs and assumes that the SCWNT length is not changed by surface exchange: e.g., to ssDNA. Atomic force microscopy (AFM) revealed a mean length of ∼1000 nm for purified ssDNA (6,5) SWCNTs and supported this assumption (Figure S3 in the Supporting Information). The fluorescence intensity for these concentration calibrated samples showed distinct differences for different ssDNA sequences (Figure 2b). $(AT)_{15}$ SWCNTs showed both the strongest emission for chirality pure and unpurified (CoMoCat) SWCNTs (Figures S4 and S5 in the Supporting Information). In contrast, $(A)_{30}$ SWCNTs showed the lowest fluorescence intensity for nonpurified CoMoCat SWCNTs but high fluorescence emission for chirality pure (6,5) SWCNTs. Distinct differences between chirality pure ssDNA (6,5) SWCNTs were also observed in terms of colloidal stability. Monochiral ssDNA SWCNTs showed a tendency to aggregation/precipitation after several days. This could be attributed to a higher purity without catalyst residues or amorphous carbon. Consequently, the stronger hydrophobic interactions between SWCNTs would cause more aggregation. Measurements over 14 days revealed a decrease in E_{11} absorbance, as well as a concomitant red shift for $(GT)_5$ (6,5) SWCNTs. In contrast, for example $(GC)_{15}$ (6,5) SWCNTs the spectra remained stable (Figure 2c and Figures S4 and S5 in the Supporting Information). Both a decrease in absorbance and red shift (broadening) are known parameters indicating SWCNT aggregation and hence loss of colloidal stability.[66]

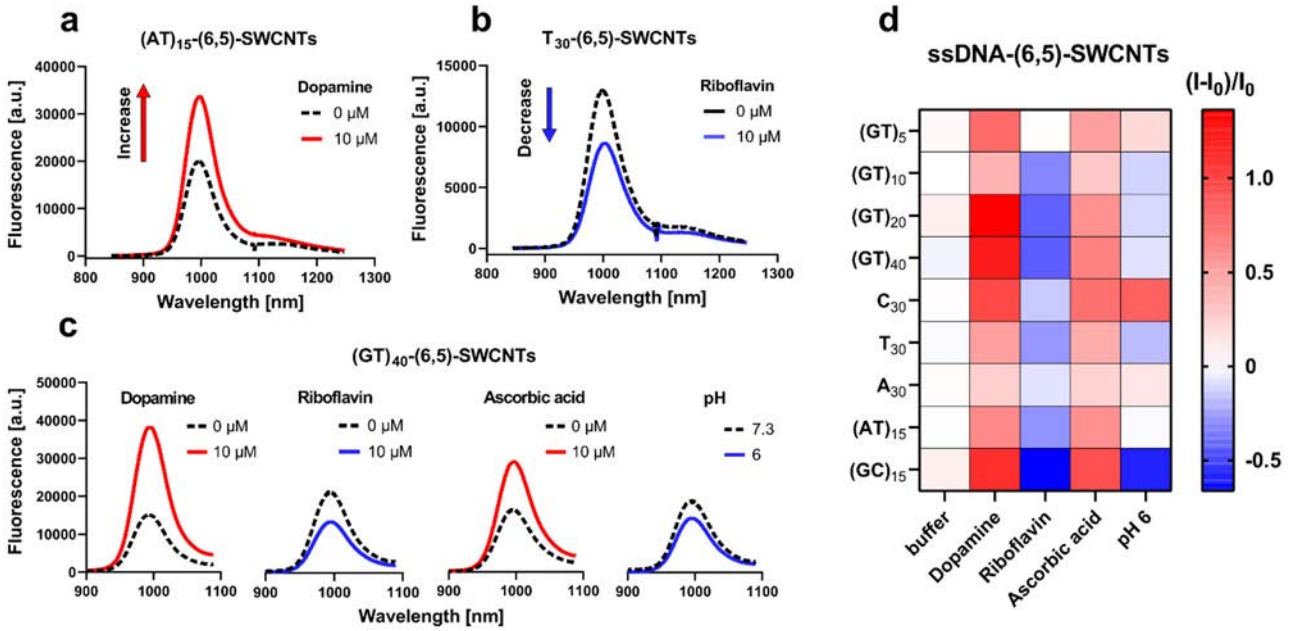

Figure 3. Sensitivity of monochiral ssDNA (6,5) SWCNT based sensors. Exemplary NIR fluorescence spectra: (a) increase in $(AT)_{15}$ (6,5) SWCNTs fluorescence in the presence of the neurotransmitter dopamine; (b) decrease in T_{30} (6,5) SWCNTs fluorescence in the presence of riboflavin; (c) fluorescence response of $(GT)_{40}$ (6,5) SWCNTs for different analytes; (d) overview of the responses of different functionalized (6,5) SWCNTs. Fluorescence increases are shown in shades of red and fluorescence decreases in shades of blue (mean, $n = 3$). The dopamine, riboflavin, and ascorbic acid concentrations are 10 μM.

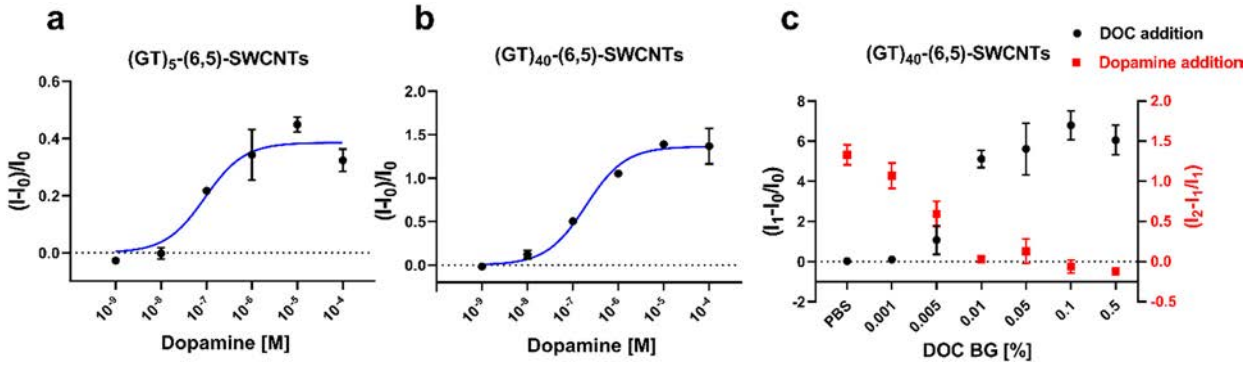

Figure 4. Sensitivity of $(GT)_x$ (6,5) SWCNT dopamine sensors and effect of surfactant residues: (a) dose dependent fluorescence response of $(GT)_5$ (6,5) SWCNT showing a maximum increase of ~40% and K_d = of 9.2 × 10^{-8} M dopamine (mean ± SEM, $n = 3$; the blue curve indicates the fit); (b) $(GT)_{40}$ (6,5) SWCNT response showing a maximum of ~140% fluorescence increase with K_d = 1.1 × 10^{-7} M dopamine (mean ± SEM, $n = 3$); (c) dopamine sensing (10 μM) with DOC background. The addition of ≥0.01% DOC (w/v) (black data points, I_1) to $(GT)_{40}$ (6,5) SWCNTs abolishes fluorescent sensing (red data points, I_2) (mean ± SEM, $n = 3$).

C_{30} and $(GC)_{15}$ (6,5) SWCNTs were the most stable sequences (Figure 2d), whereas $(GT)_5$ to $(GT)_{20}$ (6,5) SWCNTs lost >50% of the initial absorbance accompanied by a strong red shift (for more details see Figure S6 in the Supporting Information). In contrast, the longer $(GT)_{40}$ sequence showed a high colloidal stability. This result shows that the ssDNA sequence and length play a crucial role in the properties of monochiral conjugates.

Sensitivity of Monochiral Sensors. Chemical sensing with SWCNTs is a powerful tool to resolve biological processes in a spatiotemporal manner, even down to single molecule interactions.[12,17,21,67] With distinct chirality pure and hence multicolor sensors it is possible to study multiple analytes simultaneously. To mimic this scenario and rule out possible colloidal stability effects, chemical sensing of the monochiral ssDNA SWCNTs was performed after physisorption onto a glass surface.[12] Analytes that are known to modulate the fluorescence intensity of nonpurified SWCNTs in solution were added (Figure 3a,b).[58,59] The fluorescence responses for $(GT)_{40}$ (6,5) SWCNTs are highlighted in Figure 3c,d and show all sensor responses. Overall responses were similar for monochiral and multichiral ssDNA (6,5) SWCNTs, indicating that the sensing mechanism is preserved after SWCNT purification (Figure S7 in the Supporting Information). The magnitude of the fluorescence response depended on the ssDNA sequence, but no shifts in the emission peak positions were observed. In some cases, the response was stronger for nonpurified DNA SWNCTs: e.g., after 10 μM dopamine addition +120% for $(GT)_{40}$ (6,5) SWCNTs and +250% for parental $(GT)_{40}$ (CoMoCat) SWCNTs. In some cases, such as T_{30} and $(AT)_{15}$ (6,5) SWCNTs (Figure 3a and Figure S7 in the Supporting Information) the sensor response

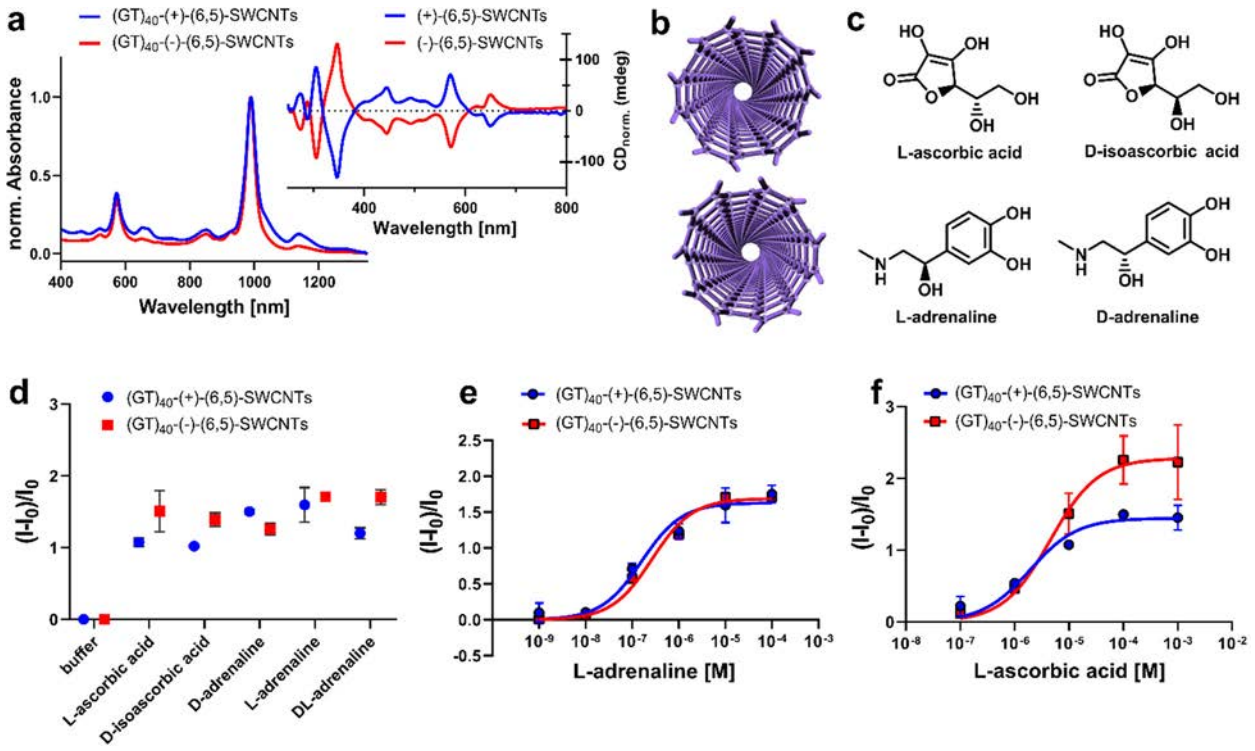

Figure 5. Sensing with (6,5) SWCNT enantiomers: (a) normalized absorbance spectra of (6,5) SWCNT enantiomers with $(GT)_{40}$ ssDNA surface modification (the inset shows the CD spectra of both (6,5) SWCNT enantiomers; (b) illustration of helical chirality of both (−) and (+) (6,5) SWCNTs; (c) tested chiral molecules; (d) fluorescence response of $(GT)_{40}$ (+) (6,5) SWCNTs and $(GT)_{40}$ (−) (6,5) SWCNTs to stereoisomers of ascorbic acid and adrenaline (mean ± SD, n = 3, analytes = 10 μM); dose−response curves of (e) L adrenaline and (f) L ascorbic acid using $(GT)_{40}$ (+) (6,5) SWCNTs and $(GT)_{40}$ (−) (6,5) SWCNTs (mean ± SD, n = 3; blue and red curves indicate fits).

was enhanced for monochiral sensors. Monochiral (6,5) SWCNTs showed an up to 10× stronger fluorescence emission (Figure S8 in the Supporting Information). The lower (relative) sensor response in some cases can be explained by the smaller room for a (relative) quantum yield increase. In general the higher brightness of monochiral SWCNTs does not lower the absolute sensor responses; however, the actual DNA confirmation might differ between purified and nonpurified SWCNT sensors.[68]

The oligonucleotide length appears to play an important role in chemical sensing and therefore dose−response curves for monochiral $(GT)_x$ (6,5) SWCNTs were collected (Figure 4a,b). The $(GT)_5$ (6,5) SWCNT response increased by +40% and saturated at ∼1 μM dopamine with a dissociation constant K_d of 9.2 × 10^{-8} M. A much stronger increase in intensity was observed for $(GT)_{40}$ (6,5) SWCNTs (+140%, saturation at ∼10 μM, K_d = 1.9 × 10^{-7} M). Furthermore, we evaluated how dopamine sensing is affected by DOC, which is a potential residue of the purification and surface exchange process.

Addition of DOC ≥0.01% (w/v) increased the fluorescence of $(GT)_{40}$ (6,5) SWCNTs (e.g. +500% for 0.01% DOC), causing a spectral (∼7 nm) blue shift and diminishing the response to dopamine (Figure 4c). A similar trend was also observed when dopamine sensing was performed 1 h after addition of DOC or when $(GT)_5$ (6,5) SWCNTs were used (Figure S9 in the Supporting Information). In turn, the red shifted peak position and the fluorescence response of ssDNA (6,5) SWCNTs to dopamine indicates that the optimized exchange procedure leaves no or a negligible amount of DOC on the SWCNT surface. These DOC addition experiments show that it abolishes sensing and (nearly) complete surfactant removal is necessary for nonbiased sensing.

Effect of SWCNT Chirality and Handedness. By using ATPE, not only specific SWCNT chiralities but also SWCNT enantiomers can be isolated.[41,45,46] We aimed to find out if the handedness itself has an effect on sensing and calls for tailored functionalization. ssDNA modified enantiomers of (6,5) SWCNTs can react differently to oxidizing agents.[49] To test chiral interactions, stereoisomers of ascorbic acid and the catecholamine adrenaline were tested. We hypothesized that the response of sensors based on enantiomerically pure SWCNTs might differ for the enantiomers of an analyte such as adrenaline.

$(GT)_{40}$ ssDNA was used for surface modification, because of its high exchange efficiency, colloidal stability, and sensor response. The enantiomeric purity, based on the CD spectra (Figure 5a) was calculated for both enantiomer fractions to be ∼80% (see Figure S10 in the Supporting Information).[69,70] Further surface exchange to $(GT)_{40}$ ssDNA yielded defined enantiomerically pure ssDNA SWCNT conjugates, used for sensing experiments (Figure 5b,c). No significant differences between the stereoisomers were found, while $(GT)_{40}$ (−) (6,5) SWCNTs reacted with a stronger response to ascorbic acid in comparison to $(GT)_{40}$ (+) (6,5) SWCNTs (Figure 5d). To rule out that fluorescence changes after analyte addition (10 μM final concentration) are biased by a possible saturation, we collected dose−response curves. The results (Figure 5e,f) indicate no difference in the response to stereoisomers of adrenaline but higher fluorescence responses for the (−) (6,5) enantiomer towards stereoisomers of ascorbic acid (see also Figure S11 in the Supporting

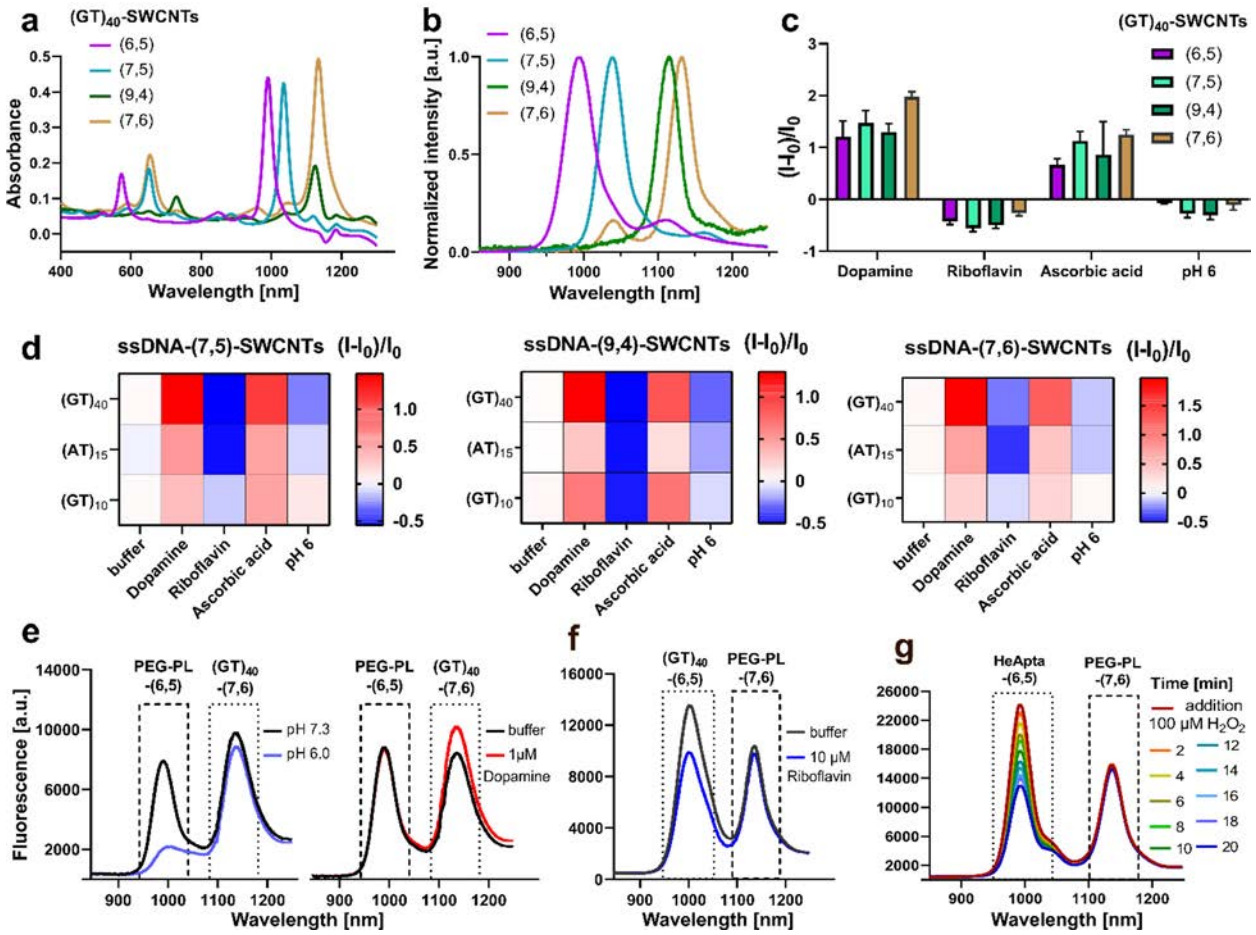

Figure 6. Multicolor and ratiometric sensing with monochiral SWCNTs: (a) absorbance spectra of different monochiral $(GT)_{40}$ SWCNTs; (b) normalized fluorescence spectra, excited at the E_{22} transition (570 nm for (6,5) SWCNTs, 650 nm for (7,5) SWCNTs, 730 nm for (9,4) SWCNTs, 650 nm for (7,6) SWCNTs); (c) similarity of the responses of monochiral $(GT)_{40}$ SWCNTs for different chiralities (mean ± SD, n = 3, c(analytes) = 10 μM); (d) fluorescence response of ssDNA (7,5) , ssDNA (9,4) , and ssDNA (7,6) SWCNT nanosensors to different analytes (mean, n = 3, analytes = 10 μM); (e) ratiometric sensing of pH change (blue) and dopamine (red) using PEG PL (6,5) SWCNTs and $(GT)_{40}$ (7,6) SWCNTs; (f) ratiometric riboflavin sensing with $(GT)_{40}$ (6,5) SWCNT and PEG PL (7,6) SWCNTs as a reference; (g) ratiometric H_2O_2 sensing with the hemin binding aptamer (HeApta) (6,5) SWCNTs and PEG PL (7,6) SWCNTs as a reference.

Information). Therefore, we conclude that the sensing and recognition mechanism (for these sensors) is not significantly affected by the handedness of the SWCNT and the chirality of these analytes. This does not rule out that other sensing mechanisms differ. Most likely, the diffusion of the exciton is affected mainly by the interaction between the analyte and the SWCNT and the chirality/band gap energy plays a minor role in the fate of the exciton. As discussed already,[49] the conformation and 3D structure of the surface adsorbed ssDNA could differ between the enantiomers[71] and might be the reason for the differences in sensing magnitudes.

Multicolor and Ratiometric Sensing. ATPE is not only feasible for (6,5) SWCNTs but also other chiralities, which opens up the possibility for nanosensors with tunable emission wavelengths. To study the effect of the SWCNT chirality on sensing, we used ATPE separated (7,5) , (9,4) , and (7,6) SWCNTs (see Figure S12 in the Supporting Information) and exchanged the surface modification again to ssDNA. This exchange process could be performed in a way similar to that shown with (6,5) SWCNTs, leading to monochiral $(GT)_{40}$ SWCNTs (Figure 6a). The distinct emission features of the used SWCNT chiralities (Figure 6b) highlight the potential for multicolor applications.

Detection of the analytes dopamine, pH, riboflavin, and ascorbic acid (Figure 6c) showed trends similar to those for monochiral (6,5) SWCNTs (Figures 6d and 3c and Figure S13 in the Supporting Information). We did not find a strong effect of SWCNT chirality on the sensor responses as has been reported in a few cases for nonpurified SWCNT samples.[72] However, the results shown in Figure 6 are the first with monochiral SWCNTs for these analytes and with well defined concentrations. In mixed samples chemical and photophysical interactions between SWCNTs of the same or different chirality might affect the fluorescence changes. From our results one can conclude that the SWCNT chirality plays a minor role in the sensitivity and mechanism of the sensors presented here. This finding does not rule out that there is a large effect of chirality for other sensor designs. However, it means that the same chemical design concepts can be applied to different chiralities, which is a big advantage. The combination of specifically modified monochiral sensors furthermore enabled ratiometric sensing (Figure 6e–g). On the basis of the variable nanosensor design (see Figures S14 and S15 in the Supporting Information) the (6,5) and the (7,6) SWCNTs can both be modified either with ssDNA (e.g., responsive to riboflavine or dopamine) or with poly(ethylene

glycol) phospholipid (PEG PL) as reference. Another ratiometric sensor detects H_2O_2 at micromolar concentrations (Figure 6g). Here, the SWCNT was modified with an aptamer that binds a protoporphyrin (hemin), which was shown to create an effective H_2O_2 sensor.[13] The choice of the reference signal is also flexible. For example, the "reference" SWCNT in ratiometric sensing can be either (6,5) or (7,6) (Figure 6e,f). Consequently, these chemical design concepts are universal and enable ratiometric sensors for multiple analytes.

DISCUSSION

Chemical sensors are powerful tools to detect biomolecules and shed light on biological processes. Fluorescent nanosensors are able to report local properties and provide the high spatial and temporal resolution that is needed to study for example cellular communication in networks of cells or even *in vivo*.[12,21,28] The biochemical complexity requires the detection of multiple analytes (multiplexing). Therefore, sensors/probes should have nonoverlapping fluorescence spectra. SWCNT based NIR fluorescent nanosensors have shown great potential to detect a range of biomolecules from neurotransmitters, reactive oxygen species, proteins, lipids, and nucleic acids.[12,13,15,24] However, in most cases the samples contained multiple chiralities of SWCNTs, which leads to congested spectra and prevents multiplexing. Additionally, it is known that the SWCNT concentration affects sensor responses due to direct and photophysical chirality dependent interactions.[20,72,73] These processes lead to a bias in sensitivity and hamper selectivity. In this work we used SWCNT purification to get close to monochiral sensors. Until now only a few studies[23,27,74] have been aimed at working with chirality pure sensors but a general concept of tunable chemical functionalization and emission wavelength was missing. This lack of progress can be explained by the experimental challenges to exchange the surface chemistry required for purification to the surface chemistry required for sensing. To obtain single SWCNT chiralities, different approaches have been developed and ATPE based protocols recently showed great potential.[41,45,46] However, even when the surface exchange of PFO sorted SWCNTs was recently established via CPEP[51] (corona phase exchange purification), most protocols stop when it comes to a modular surface chemistry beyond typical surfactants. We modified and optimized a DOC to ssDNA exchange process[60] and used the commercially available PEG (6 kDa) as the polymer.

For monochiral SWCNTs immobilized on a surface, we found the strongest dopamine responses for $(GT)_{40}$ SWCNTs. Most other studies in the literature used mixed chirality SWCNT sensors in solution. In contrast, nonspecific interactions or aggregation is minimized on a surface. The evaluated K_d value for $(GT)_{40}$ (6,5) SWCNTs of 190 nM outlines the potential for neurotransmitter imaging in fast biological prosesses.[28] Additionally, we studied to our knowledge for the first time enantiomerically pure ssDNA SWCNTs for sensing. No significant difference was observed for the chiral catecholamine adrenaline, indicating that the analyte sensing and recognition mechanism is not affected by the stereochemical conformation of the small molecules. Our results also indicate that the handedness of the SWCNT does not change the sensing mechanism, at least for these catecholamine sensors. The current understanding is that the interaction between the catechol moiety and the phosphate backbone leads to conformational changes that affect exciton dynamics.[12] It is also known that the direct chemical environment can change the exciton diffusion substantially.[75] This indicates that changes in the surface chemistry affect exciton dynamics but do not necessarily depend on the stereochemistry. Consequently, the chiral part of the catechol amines plays a less important role. On the basis of these results one can conclude that mixed enantiomer samples do not reduce sensor performance. However, it does not rule out that for other sensing mechanisms the handedness of the SWCNT itself plays a different role.

Sensing with (7,5), (9,4), and (7,6) SWCNTs showed qualitatively results very similar to those for for ssDNA (6,5) SWCNTs: e.g. a 120−190% fluorescence increase for $(GT)_{40}$ SWCNTs after dopamine addition. It is known that the fluorescence response to analytes is influenced by the SWCNT sensor concentration, and therefore we performed these experiments with exactly the same SWCNT concentrations.[73] These experiments are the first ones outside of mixtures and report fluorescence changes in a well defined system. They provide a much clearer picture of the effect of the heterogeneity of nanomaterials on their function. The developed approach to exchange the coating DOC of chirality pure SWCNTs to a biopolymer is feasible for all kinds of chirality pure samples (Figure 6). From these large scale and stable stock solutions, various sensors can be created by methanol based exchange,[60] which opens up the possibilities to all desirable combinations of SWCNT chiralities (emission features) and diverse surface modifications (sensing and recognition units). Technical and conceptual challenges have so far prevented the preparation of tunable monochiral sensors. In our work we show the potential and difficulties such as surfactant residues (Figure 3) in the preparation of monochiral SWCNT based sensors. These results indicate that the surface chemistry creates the different sensing responses and enables a predictable design concept. Additionally, the nonoverlapping spectra allow a combination of multiple sensors in ratiometric and multiplexed approaches, which increases the selectivity and robustness in imaging. These advances will help to increase sensing performance for example when neurotransmitter release from cells is imaged.[12,21]

CONCLUSION

In summary, we systematically studied the properties of monochiral ssDNA SWCNT NIR fluorescent sensors. We developed a robust surface functionalization exchange process and show how the ssDNA sequence and length affects the colloidal stability, photophysics, and sensing. These functional SWCNTs allowed us to gain insights into the effects of chirality, handedness, and residues from SWCNT separation on the sensitivity of sensors for multiple analytes. Consequently, NIR ratiometric sensors for the important analytes dopamine, riboflavin, and H_2O_2 or pH changes were demonstrated. These conceptual and mechanistic insights pave the way for tailored multicolor and ratiometric biosensing and imaging applications.

AUTHOR INFORMATION

Corresponding Author

Sebastian Kruss − *Institute of Physical Chemistry, Göttingen University, 37077 Göttingen, Germany; Physical Chemistry II, Bochum University, 44801 Bochum, Germany; Fraunhofer Institute for Microelectronic Circuits and Systems, 47057 Duisburg, Germany;* ; Email: sebastian.kruss@rub.de

Authors

Robert Nißler − *Institute of Physical Chemistry, Göttingen University, 37077 Göttingen, Germany; Physical Chemistry II, Bochum University, 44801 Bochum, Germany;*

Larissa Kurth − *Institute of Physical Chemistry, Göttingen University, 37077 Göttingen, Germany*

Han Li − *Institute of Nanotechnology, Karlsruhe Institute of Technology (KIT), 76344 Eggenstein Leopoldshafen, Germany*

Alexander Spreinat − *Institute of Physical Chemistry, Göttingen University, 37077 Göttingen, Germany*

Ilyas Kuhlemann − *Institute of Physical Chemistry, Göttingen University, 37077 Göttingen, Germany*

Benjamin S. Flavel − *Institute of Nanotechnology, Karlsruhe Institute of Technology (KIT), 76344 Eggenstein Leopoldshafen, Germany;*

Author Contributions

R.N. and S.K. designed and conceived the research. S.K. coordinated the project. L.K. and R.N. separated (6,5) SWCNTs and performed and characterized surface exchange and chemical sensing experiments, R.N. performed AFM experiments, A.S. and I.K. wrote Python based analysis scripts for absorbance and sensing evaluation. H.L. and B.S.F. separated (7,5) , (9,4) , and (7,6) SWCNTs and enantiomers of (6,5) SWCNTs. All authors contributed to the writing of the manuscript and analysis of data. All authors have given approval to the final version of the manuscript.

Notes

The authors declare no competing financial interest.

ACKNOWLEDGMENTS

This project was supported by the VW foundation. Funded by the Deutsche Forschungsgemeinschaft (DFG, German Research Foundation) under Germany's Excellence Strategy − EXC 2033 − 390677874 − RESOLV. We thank the DFG for funding within the Heisenberg program (B.S.F. and S.K.). We thank Gabriele Selvaggio for help with AFM measurements.

ABBREVIATIONS

SWCNT, single wall carbon nanotubes; NIR, near infrared; ATPE, aqueous two phase extraction; DOC, sodium deoxycholate; ssDNA, single stranded DNA; PEG PL, poly(ethylene glycol) phospholipid

REFERENCES

(1) Li, J.; Pandey, G. P. *Annu. Rev. Phys. Chem.* **2015**, *66* (1), 331−356.

(2) Zamolo, V. Z.; Vazquez, E.; Prato, M. *Top. Curr. Chem.* **2013**, *286*, 1−72.

(3) Nanot, S.; Hároz, E. H.; Kim, J. H.; Hauge, R. H.; Kono, J. O. *Adv. Mater.* **2012**, *24* (36), 4977−4994.

(4) Amori, A. R.; Hou, Z.; Krauss, T. D. *Annu. Rev. Phys. Chem.* **2018**, *69* (1), 81−100.

(5) O'Connell, M. J.; Bachilo, S. M.; Huffman, C. B.; Moore, V. C.; Strano, M. S.; Haroz, E. H.; Rialon, K. L.; et al. *Science* **2002**, *297* (5581), 593−596.

(6) Bachilo, S. M.; Strano, M. S.; Kittrell, C.; Hauge, R. H.; Smalley, R. E.; Weisman, R. B. *Science* **2002**, *298*, 2361−2367.

(7) Kruss, S.; Hilmer, A. J.; Zhang, J.; Reuel, N. F.; Mu, B.; Strano, M. S. *Adv. Drug Delivery Rev.* **2013**, *65* (15), 1933−1950.

(8) Hong, G.; Diao, S.; Antaris, A. L.; Dai, H. *Chem. Rev.* **2015**, *115* (19), 10816−10906.

(9) Farrera, C.; Torres Andón, F.; Feliu, N. C. *ACS Nano* **2017**, *11* (11), 10637−10643.

(10) Hendler Neumark, A.; Bisker, G. *Sensors* **2019**, *19* (24), 5403.

(11) Dinarvand, M.; Elizarova, S.; Daniel, J.; Kruss, S. *ChemPlusChem* **2020**, *85* (7), 1465−1480.

(12) Kruss, S.; Salem, D. P.; Vuković, L.; Lima, B.; Vander Ende, E.; Boyden, E. S.; Strano, M. S. *Proc. Natl. Acad. Sci. U. S. A.* **2017**, *114* (8), 1789−1794.

(13) Wu, H.; Nißler, R.; Morris, V.; Herrmann, N.; Hu, P.; Jeon, S.; Kruss, S.; Giraldo, J. P. *Nano Lett.* **2020**, *20* (4), 2432−2442.

(14) Lew, T. T. S.; Koman, V. B.; Silmore, K. S.; Seo, J. S.; Gordiichuk, P.; Kwak, S. Y.; Park, M.; et al. *Nat. Plants* **2020**, *6* (4), 404−415.

(15) Harvey, J. D.; Jena, P. V.; Baker, H. A.; Zerze, G. H.; Williams, R. M.; Galassi, T. V.; Roxbury, D.; Mittal, J.; Heller, D. A. *Nat. Biomed. Eng.* **2017**, *1* (4), 1−43.

(16) Williams, R. M.; Lee, C.; Galassi, T. V.; Harvey, J. D.; Leicher, R.; Sirenko, M.; Dorso, M. A.; Shah, J.; Olvera, N.; Dao, F. *Sci. Adv.* **2018**, *4* (4), eaaq1090.

(17) Kim, J. H.; Heller, D. A.; Jin, H.; Barone, P. W.; Song, C.; Zhang, J.; Trudel, L. J.; Wogan, G. N.; Tannenbaum, S. R.; Strano, M. S. *Nat. Chem.* **2009**, *1* (6), 473−481.

(18) Gravely, M.; Safaee, M. M.; Roxbury, D. *Nano Lett.* **2019**, *19* (9), 6203−6212.

(19) Beyene, A. G.; Delevich, K.; Del Bonis O'Donnell, J. T.; Piekarski, D. J.; Lin, W. C.; Thomas, A. W.; et al. *Sci. Adv.* **2019**, *5* (7), eaaw3108.

(20) Kruss, S.; Landry, M. P.; Vander Ende, E.; Lima, B. M. A.; Reuel, N. F.; Zhang, J.; Nelson, J.; Mu, B.; Hilmer, A.; Strano, M. *J. Am. Chem. Soc.* **2014**, *136* (2), 713−724.

(21) Dinarvand, M.; Neubert, E.; Meyer, D.; Selvaggio, G.; Mann, F. A.; Erpenbeck, L.; Kruss, S. *Nano Lett.* **2019**, *19* (9), 6604−6611.

(22) Harvey, J. D.; Baker, H. A.; Ortiz, M. V.; Kentsis, A.; Heller, D. *ACS Sensors* **2019**, *4* (5), 1236−1244.

(23) Galassi, T. V.; Jena, P. V.; Shah, J.; Ao, G.; Molitor, E.; Bram, Y.; Frankel, A.; Park, J.; Jessurun, J.; Ory, D. S.; et al. *Sci. Transl. Med.* **2018**, *10* (461), eaar2680.
(24) Bisker, G.; Dong, J.; Park, H. D.; Iverson, N. M.; Ahn, J.; Nelson, J. T.; Landry, M. P.; Kruss, S.; Strano, M. S. *Nat. Commun.* **2016**, *7*, 1−14.
(25) Bisker, G.; Bakh, N. A.; Lee, M. A.; Ahn, J.; Park, M.; O'Connell, E. B.; Iverson, N. M.; Strano, M. S. *ACS Sensors* **2018**, *3* (2), 367−377.
(26) Zubkovs, V.; Schuergers, N.; Lambert, B.; Ahunbay, E.; Boghossian, A. A. *Small* **2017**, *13* (42), 1701654.
(27) Nißler, R.; Bader, O.; Dohmen, M.; Walter, S. G.; Noll, C.; Selvaggio, G.; Groß, U.; Kruss, S. *Nat. Commun.* **2020**, *11* (1), 1−12.
(28) Meyer, D.; Hagemann, A.; Kruss, S. *ACS Nano* **2017**, *11* (4), 4017−4027.
(29) Wang, J. Q.; Ding, F.; Luo, D.; Zhang, D.; Wang, X.; Yang, J.; Bai, X.; Peng, F.; Xu, Z.; Wei, J.; et al. *Nature* **2014**, *510* (7506), 522−524.
(30) An, H.; Kumamoto, A.; Takezaki, H.; Ohyama, S.; Qian, Y.; Inoue, T.; Ikuhara, Y.; Chiashi, S.; Xiang, R.; Maruyama, S. *Nanoscale* **2016**, *8* (30), 14523−14529.
(31) Yang, F.; Wang, M.; Zhang, D.; Yang, J.; Zheng, M.; Li, Y. *Chem. Rev.* **2020**, *120* (5), 2693−2758.
(32) Zheng, M. *Top. Curr. Chem.* **2017**, *375* (1), 1−36.
(33) Arnold, M. S.; Green, A. A.; Hulvat, J. F.; Stupp, S. I.; Hersam, M. C. *Nat. Nanotechnol.* **2006**, *1* (1), 60−65.
(34) Ghosh, S.; Bachilo, S. M.; Weisman, R. B. *Nat. Nanotechnol.* **2010**, *5* (6), 443−450.
(35) Liu, H.; Nishide, D.; Tanaka, T.; Kataura, H. *Nat. Commun.* **2011**, *2*, 1−8.
(36) Flavel, B. S.; Kappes, M. M.; Krupke, R.; Hennrich, F. *ACS Nano* **2013**, *4*, 3557−3564.
(37) Tvrdy, K.; Jain, R. M.; Han, R.; Hilmer, A. J.; Mcnicholas, T. P.; Strano, M. S. *ACS Nano* **2013**, *7*, 1779−1789.
(38) Tu, X.; Manohar, S.; Jagota, A.; Zheng, M. *Nature* **2009**, *460* (7252), 250−253.
(39) Fagan, J. A.; Khripin, C. Y.; Silvera Batista, C. A.; Simpson, J. R.; Hároz, E. H.; Hight Walker, A. R.; Zheng, M. *Adv. Mater.* **2014**, *26* (18), 2800−2804.
(40) Khripin, C. Y.; Fagan, J. A.; Zheng, M. *J. Am. Chem. Soc.* **2013**, *135* (18), 6822−6825.
(41) Li, H.; Gordeev, G.; Garrity, O.; Reich, S.; Flavel, B. S. *ACS Nano* **2019**, *13*, 2567−2578.
(42) Zheng, M.; Jagota, A.; Strano, M. S.; Santos, A. P.; Barone, P.; Chou, S. G.; Diner, B. A.; Dresselhaus, M. S.; Mclean, R. S.; Onoa, G. B.; et al. *Science* **2003**, *302*, 1545−1549.
(43) Zheng, M.; Jagota, A.; Semke, E. D.; Diner, B. A.; McLean, R. S.; Lustig, S. R.; Richardson, R. E.; Tassi, N. G. *Nat. Mater.* **2003**, *2* (5), 338−342.
(44) Nish, A.; Hwang, J. Y.; Doig, J.; Nicholas, R. J. *Nat. Nanotechnol.* **2007**, *2* (10), 640−646.
(45) Fagan, J. A. *Nanoscale Adv.* **2019**, *1* (9), 3307−3324.
(46) Li, H.; Gordeev, G.; Garrity, O.; Peyyety, N. A.; Selvasundaram, P. B.; Dehm, S.; Krupke, R.; Cambré, S.; Wenseleers, W.; Reich, S.; et al. *ACS Nano* **2020**, *14* (1), 948−963.
(47) Wei, L.; Flavel, B. S.; Li, W.; Krupke, R.; Chen, Y. *Nanoscale* **2017**, *9* (32), 11640−11646.
(48) Sims, C. M.; Fagan, J. *Carbon* **2020**, *165*, 196−203.
(49) Ao, G.; Streit, J. K.; Fagan, J. A.; Zheng, M. *J. Am. Chem. Soc.* **2016**, *138* (51), 16677−16685.
(50) Lyu, M.; Meany, B.; Yang, J.; Li, Y.; Zheng, M. *J. Am. Chem. Soc.* **2019**, *141* (51), 20177−20186.
(51) Nißler, R.; Mann, F. A.; Preiß, H.; Selvaggio, G.; Herrmann, N.; Kruss, S. *Nanoscale* **2019**, *11* (23), 11159−11166.
(52) Mann, F. A.; Horlebein, J.; Meyer, N. F.; Meyer, D.; Thomas, F.; Kruss, S. *Chem. Eur. J.* **2018**, *24*, 12241−12245.
(53) Polo, E.; Nitka, T.; Neubert, E.; Erpenbeck, L.; Vuković, L.; Kruss. *ACS Appl. Mater. Interfaces* **2018**, *10*, 17693−17703.
(54) Mann, F. A.; Lv, Z.; Grosshans, J.; Opazo, F.; Kruss, S. *Angew. Chem., Int. Ed.* **2019**, *58*, 11469−11473.
(55) Welsher, K.; Liu, Z.; Sherlock, S. P.; Robinson, J. T.; Chen, Z.; Daranciang, D.; Dai, H. *Nat. Nanotechnol.* **2009**, *4* (11), 773−780.
(56) Mann, F. A.; Herrmann, N.; Opazo, F.; Kruss, S. *Angew. Chem., Int. Ed.* **2020**, *59*, 11732−11738.
(57) Mann, F. A.; Herrmann, N.; Meyer, D.; Kruss, S. *Sensors* **2017**, *17*, 1521.
(58) Polo, E.; Kruss, S. *J. Phys. Chem. C* **2016**, *120* (5), 3061−3070.
(59) Nißler, R.; Mann, F. A.; Chaturvedi, P.; Horlebein, J.; Meyer, D.; Vukovic, L.; Kruss, S. *J. Phys. Chem. C* **2019**, *123*, 4837−4847.
(60) Streit, J. K.; Fagan, A.; Zheng, M. *Anal. Chem.* **2017**, *89*, 10496−10503.
(61) Pan, J.; Zhang, H.; Cha, T. G.; Chen, H.; Choi, J. H. *Anal. Chem.* **2013**, *85* (17), 8391−8396.
(62) Streit, J. K.; Bachilo, S. M.; Ghosh, S.; Lin, C.; Weisman, R. B. *Nano Lett.* **2014**, *14*, 1530−1536.
(63) Sanchez, S. R.; Bachilo, S. M.; Kadria Vili, Y.; Lin, C. W.; Weisman, R. B. *Nano Lett.* **2016**, *16* (11), 6903−6909.
(64) Schöppler, F.; Mann, C.; Hain, T. C.; Neubauer, F. M.; Privitera, G.; Bonaccorso, F.; Chu, D.; Ferrari, A. C.; Hertel, T. *J. Phys. Chem. C* **2011**, *115* (30), 14682−14686.
(65) Zhang, J.; Landry, M. P.; Barone, P. W.; Kim, J. H.; Lin, S.; Ulissi, Z. W.; Lin, D.; Mu, B.; Boghossian, A. A.; Hilmer, A. J.; et al. *Nat. Nanotechnol.* **2013**, *8* (12), 959−968.
(66) O'Connell, M.; Bachilo, S.; Huffman, C.; Moore, C.; et al. *Science* **2002**, *297*, 593−596.
(67) Meyer, D.; Telele, S.; Zelená, A.; Gillen, A. J.; Antonucci, A.; Neubert, E.; Nißler, R.; Boghossian, A. A.; et al. *Nanoscale* **2020**, *12*, 9104−9115.
(68) Yang, Y.; Sharma, A.; Noetinger, G.; Zheng, M.; Jagota, A. *J. Phys. Chem. C* **2020**, *124* (16), 9045−9055.
(69) Sato, N.; Tatsumi, Y.; Saito, R. *Phys. Rev. B* **2017**, *95* (15), 1−11.
(70) Wei, X.; Tanaka, T.; Hirakawa, T.; Yomogida, Y.; Kataura, H. *J. Am. Chem. Soc.* **2017**, *139* (45), 16068−16071.
(71) Zheng, Y.; Alizadehmojarad, A. A.; Bachilo, S. M.; Kolomeisky, A. B.; Weisman, R. B. *ACS Nano* **2020**, *14* (9), 12148−12158.
(72) Salem, D. P.; Landry, M. P.; Bisker, G.; Ahn, J.; Kruss, S.; Strano, M. S. *Carbon* **2016**, *97*, 147−153.
(73) Landry, M. P.; Vukovic, L.; Kruss, S.; Bisker, G.; Landry, A. M.; Islam, S.; Jain, R.; Schulten, K.; Strano, M. S. *J. Phys. Chem. C* **2015**, *119*, 10048−10058.
(74) Giraldo, J. P.; Landry, M. P.; Kwak, S. Y.; Jain, R. M.; Wong, M. H.; Iverson, N. M.; Ben Naim, M.; Strano, M. S. *Small* **2015**, *11* (32), 3973−3984.
(75) Siitonen, A. J.; Tsyboulski, D. A.; Bachilo, S. M.; Weisman, R. *Nano Lett.* **2010**, *10* (5), 1595−1599.